Local Transfer Function, Stability, and Empirical Frequency Response of a Nonlinear SISO System

TargetDeLab Technical Paper 02

TargetDeLab Group

2026

Abstract

This study re-examines the frequency-domain description and stability of a nonlinear SISO system of the form $\dot{x} = f(x) + u$, y=x. A naive formulation would treat Fourier ratios X/U as exact transfer functions of the nonlinear plant. A classical transfer function can be defined only for the local linearization about an equilibrium point, whereas spectral ratios obtained from finite experiments are defined as empirical, experiment-dependent frequency responses. For the nominal model $\dot{x} = x^2 + u$, the local result is $P_{\text{lin}}(s; x_e)$=1/(s-2x_e), giving the familiar $1/s$ form at $x_e = 0$. In parallel, the notion of "attainable stability" is reformulated as local stabilizability of the equilibrium point. Six simulation families examine PID gains, numerical convergence, reference-signal bandwidth, nonlinearity order, dependence of the empirical FRF on excitation amplitude, and local stabilizability. The results confirm that $1/s$ behavior is correct as a small-signal description at $x_e = 0$, not as a unique global transfer function of the nonlinear system.

Keywords: nonlinear systems, local linearization, empirical frequency response, multisine, nonlinear distortion, PID, stabilizability, system identification.

1 Introduction and Literature Context

The use of transfer functions and Bode diagrams relies on linearity and time invariance. In a nonlinear system, superposition does not hold and periodic excitation may generate harmonics and intermodulation terms. Consequently, a single output-to-input ratio in the frequency domain is generally not an intrinsic plant property independent of the experiment.

Classical nonlinear control theory uses local Jacobian linearization, Lyapunov analysis, and phase-space tools to draw stability conclusions [1,2]. In frequency-domain identification, Pintelon and Schoukens systematically introduce the Best Linear Approximation (BLA) and multisine excitation techniques for detecting nonlinear distortion [3-5]. Volterra series and generalized/nonlinear output frequency-response

functions provide genuine higher-order nonlinear frequency descriptions [6-8].

This chapter extracts useful frequency-domain information from a nonlinear SISO system while strictly separating three distinct concepts: (i) a local classical transfer function obtained by linearization, (ii) an empirical FRF obtained from a specific excitation and time window, and (iii) higher-order nonlinear frequency representations, which are discussed in the literature but are not required for the basic experiments of this study.

1.1 Transfer Functions as Linear Time-Invariant Objects

For an LTI system with zero initial conditions, the input-output relation is a convolution y(t)=(g*u)(t). The Laplace transform converts convolution into multiplication, yielding Y(s)=G(s)U(s), where the transfer function G(s) depends on the system but not on the particular input used to probe it. This input-independence follows directly from linearity and time invariance. In a nonlinear system, superposition is lost: the response to u1+u2 is generally not the sum of the responses to u1 and u2, and scaling the input can alter both the magnitude and the spectral content of the output. A single global transfer function therefore cannot, in general, represent the nonlinear input-output map [1,2,10].

The absence of a global nonlinear transfer function does not remove the usefulness of frequency-domain reasoning. It requires a more precise statement of what has been measured or approximated. Three useful levels are distinguished in this book: a local transfer function of a linearized model, an experiment-dependent empirical frequency response, and a higher-order nonlinear frequency representation such as a Volterra or output-frequency-response description [3,6-8].

1.2 Equilibria, Linearization, and the Local Small-Signal Model

Consider a smooth nonlinear system $\dot{x}$=F(x,u), y=H(x,u) and an equilibrium (x_e,u_e) satisfying F(x_e,u_e)=0. For small perturbations δx=x-x_e and δu=u-u_e, a first-order Taylor expansion gives $\delta\dot{x}$=A δx+B δu plus higher-order terms, with A and B equal to the Jacobians of F at the equilibrium. The corresponding output equation is δy=C δx+D δu plus higher-order terms. Neglecting second- and higher-order terms produces an LTI small-signal model whose transfer matrix is $C(sI - A)^{-1}B + D$ [1,2,10-11].

The approximation is local in state, input, and operating point. Its validity is controlled by the magnitude of the neglected higher-order terms and by the time interval over which the perturbed trajectory remains in the neighborhood where the Taylor model is accurate. A local Bode diagram therefore answers a precise question: how do sufficiently small perturbations behave near a specified equilibrium? It does not describe finite-amplitude excursions throughout the nonlinear state space.

1.3 Local Stability, Hyperbolicity, and Stabilizability

For a continuously differentiable autonomous system $\dot{x}$=f(x), linearization about an equilibrium can often determine local stability when the Jacobian has no eigenvalues on the imaginary axis. If all eigenvalues have negative real part, the equilibrium is locally exponentially stable; if at least one eigenvalue has positive real part, it is unstable. When eigenvalues lie on the imaginary axis, linearization alone is inconclusive and nonlinear tools such as Lyapunov functions, center-manifold analysis, or normal-form arguments may be required [1,10-11]. This is why the equilibrium x_e=0 of $\dot{x}$=x^2 is called nonhyperbolic rather than automatically stable or unstable by the linear test alone.

Stabilizability is a control property rather than an open-loop stability property. For the local pair (A,B), stabilizability requires every uncontrollable mode to be stable; when the scalar input coefficient is nonzero, proportional or dynamic feedback may shift the controllable local pole. The chapter uses this standard local concept in place of the nonstandard phrase 'attainable stability'.

1.4 Empirical Frequency Responses and Best Linear Approximation

A measured spectral ratio is meaningful only where the input provides sufficient excitation and where transient, leakage, noise, and nonlinear-distortion effects are controlled. Periodic multisines are particularly useful because they permit selected frequency lines to be excited while leaving other lines unexcited. Energy appearing at unexcited detection lines then provides direct evidence of nonlinear distortion. Random-phase multisines additionally support statistically meaningful linear approximations over an excitation class [3-5].

The Best Linear Approximation is the linear model that minimizes a specified mean-square discrepancy for a defined class of random or periodic excitations. Because the optimum depends on the excitation statistics, amplitude distribution, operating condition, and feedback configuration, a BLA is not an intrinsic global transfer function of the nonlinear plant [3,5,12]. This dependence is not a defect: it makes the approximation explicitly conditional and therefore scientifically interpretable. The empirical FRF used in this chapter is a simpler experiment-specific object; the simulation studies show when it approaches the local small-signal model and when amplitude dependence becomes visible.

2 Theoretical Formulation

Plant and control topology used in this chapter. The nonlinear SISO plant $\dot{x} = f(x)+u$, y=x is operated in feedback when closed-loop tracking is studied. Local transfer functions are formed only after linearization about (x_e,u_e); empirical FRFs are obtained from separately specified excitation experiments and are not inserted as intrinsic plant blocks.

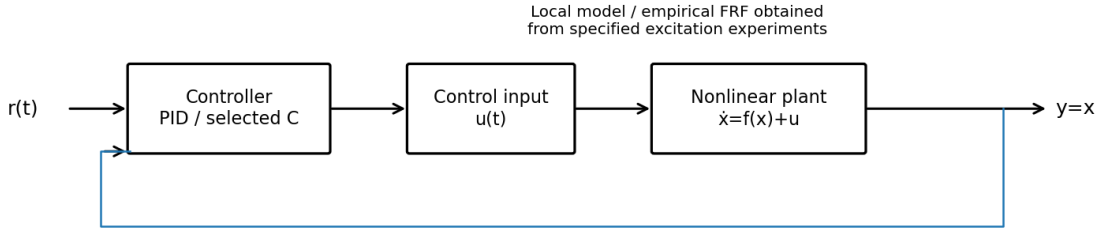


Figure 8. Control topology used in Chapter 2.

2.1 Nonlinear Model and Equilibrium Points

Consider the scalar SISO model

$$\dot{x}(t) = f(x(t)) + u(t),\ y(t)=x(t) \tag{1}$$

with f continuously differentiable in the operating region. An equilibrium point (x_e,u_e) satisfies

$$0 = f(x_e) + u_e \Rightarrow u_e = -f(x_e) \tag{2}$$

2.2 Local Transfer Function

Let δx=x-x_e and δu=u-u_e and expand to first order:

$$\delta\dot{x} = a\delta x + \delta u + O(\delta x^2),\ a = f'(x_e) \tag{3}$$

The first-order approximation gives an LTI small-signal model. With zero initial conditions, the local transfer function is

$$P_{\text{lin}}(s;x_e) = \Delta X(s)/\Delta U(s) = 1/(s-a) \tag{4}$$

This is the only classical transfer function used in the study. It is local: it depends on the operating point through a=f'(x_e).

2.2.1 2.3.3. Special Case f(x)=x^2

$$\dot{x} = x^2 + u \tag{5}$$

$$u_e = -x_e^2,\ a = 2x_e,\ P_{\text{lin}}(s;x_e)=1/(s-2x_e) \tag{6}$$

At x_e=0, P_{lin}(s;0)=$1/s$. Thus the -20 dB/decade slope observed in the observed behavior has a clear and correct interpretation: it is the small-signal limit about the zero operating point. It does not prove a global transfer function equal to $1/s$.

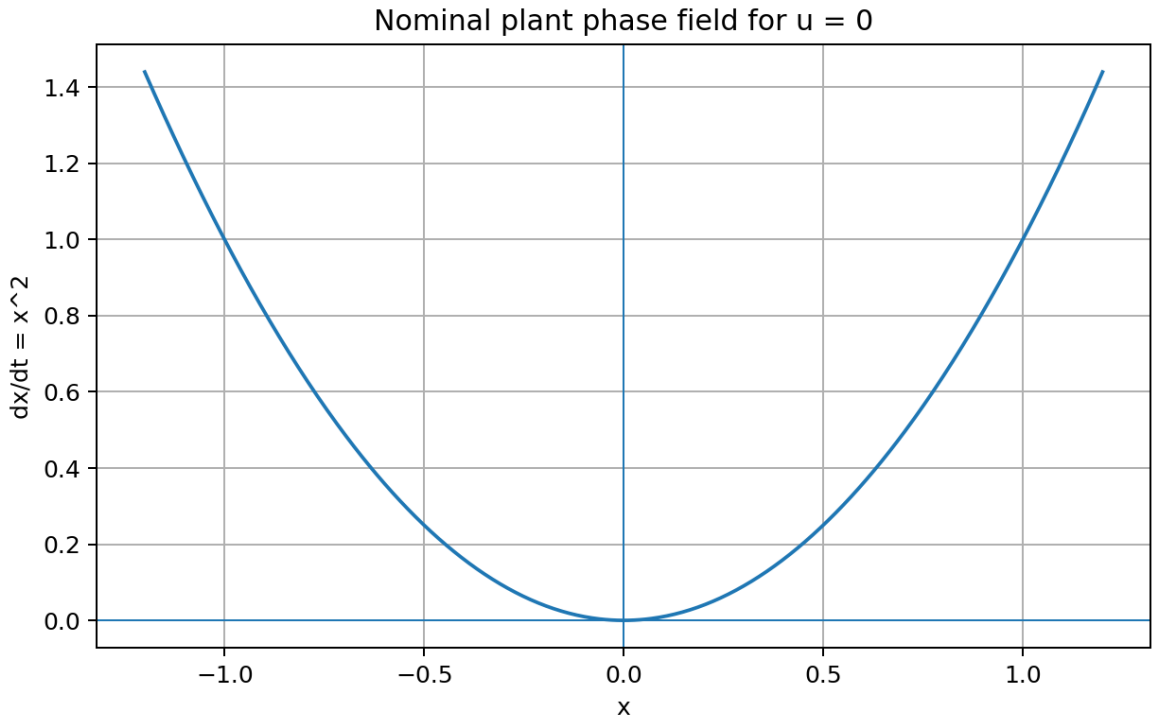


Figure 9. Phase field of the nominal plant $\dot{x}$=x^2 for u=0.

2.3 Local Stability and "Attainable Stability"

For the local open-loop system $\delta\dot{x}$=a δx, the equilibrium is locally asymptotically stable for $a < 0$, unstable for $a > 0$, and nonhyperbolic for a=0. For f=x^2 this means $x_e < 0$ is stable, $x_e > 0$ is unstable, and x_e=0 is nonhyperbolic.

The relevant concept is formulated as local stabilizability: there exists a controller that makes the linearized closed-loop system Hurwitz. With proportional feedback δu=-K δx,

$$\delta\dot{x} = (a\text{-}K)\delta x \tag{7}$$

$$K > a \Rightarrow \text{local asymptotic stability} \tag{8}$$

With an ideal PID C(s)=Kp+Kd s+Ki/s and P_{lin}=1/(s-a), the characteristic equation becomes

$$(1+K_d)s^2 + (K_p\text{-}a)s + K_i = 0 \tag{9}$$

For a second-order polynomial, necessary and sufficient Hurwitz conditions are 1+Kd>0, Kp-$a > 0$, and Ki>0.

2.4 Empirical Frequency Response

For a specified experiment E={u(t),x(0),T,dt,level,phases}, define at the excited frequencies ω_k only the experiment-dependent quantity

$$G_E(\mathrm{j}\omega_\mathrm{k}) = X_E(\mathrm{j}\omega_\mathrm{k}) \,/\, U_E(\mathrm{j}\omega_\mathrm{k}),\ |U_E(\mathrm{j}\omega_\mathrm{k})| > \varepsilon \tag{10}$$

G_E is not a unique transfer function of the nonlinear plant. It changes with the level and spectral content of u, the operating point, the time window, and the initial conditions. In the small-signal limit, provided the linearization is valid, G_E approaches $P_{\mathrm{lin}}(\mathrm{j}\ \omega)$.

2.5 Nonlinear Spectral-Distortion Index

For the quadratic model, a multisine is used that excites only odd integer lines 1,3,...,99 Hz. The even lines 2,4,...,198 Hz are absent from the input and act as detection lines for quadratic distortion. Define

$$D_{\mathrm{even}} = \sqrt{\frac{\sum_{k\in\mathcal{K}_{\mathrm{even}}} |X(k)|^2}{\sum_{k\in\mathcal{K}_{\mathrm{excited}}} |X(k)|^2}} \tag{11}$$

The index is not claimed to be a complete BLA estimator; it is used here as a simple reproducible indicator of nonlinear energy at unexcited even lines.

3 Computational Methodology

The numerical study employs fourth-order Runge-Kutta (RK4) integration of the plant with zero-order hold on u at each sample. The PID is implemented discretely, with rectangular integration and a finite difference for the derivative term.

Performance is assessed using the metrics defined in the Mathematical Nomenclature.

4 Simulation Scenarios and Results

4.1 Scenario 1 - Effect of PID Gains

Scenario definition. The nominal plant is $\dot{x} = x^2 + u$ with x(0)=0 and the accelerated reference $r(t) = 5t^2$ for $0 \le t < 0.5$ s, followed by the constant value 1.25. With Δt=10^{-4} s, four gain sets are applied: (Kp,Kd,Ki)=(5,0.002,7.5), (25,0.01,37.5), (50,0.02,75), and (500,0.2,750). Only the PID gains are changed.

The accelerated reference $r(t) = 5t^2$ for $0 \le t < 0.5$ s followed by the constant value 1.25 is retained. The nominal plant is $\dot{x} = x^2 + u$ and dt=10^{-4} s. The corresponding numerical results are summarized in Table 3.

Table 5. Scenario 1 results.

ID	K_p	K_d	K_i	Exit	IAE	RMSE	E_u	$\lvert u\rvert_{\max}$
1a	5	0.002	7.5	0.57031	0.267599	0.318838	3.07974	3.48015
1b	25	0.01	37.5	0.0637621	0.0743976	0.0807339	4.53744	3.80313
1c	50	0.02	75	0.0289405	0.0371696	0.0397965	4.40019	3.64912
1d	500	0.2	750	0.00270113	0.00369678	0.00390806	4.23762	3.49817

Increasing the gains drastically reduces the error: IAE decreases from 0.2676 to 0.003697, while control energy remains of order 3-4.5 for this particular smooth reference signal. This observation concerns closed-loop performance, not a change in a “transfer function” of the nonlinear plant.

This gain sweep separates tracking accuracy from the plant-description question. The monotonic reduction in IAE demonstrates that the closed-loop trajectory can be made progressively tighter by increasing the PID gains for this smooth command, while the relatively moderate change in Eu shows that the particular reference does not strongly excite the derivative channel. The result therefore characterizes controller tuning for this experiment; it does not imply that the nonlinear plant itself has acquired a different frequency response when the gains are changed.

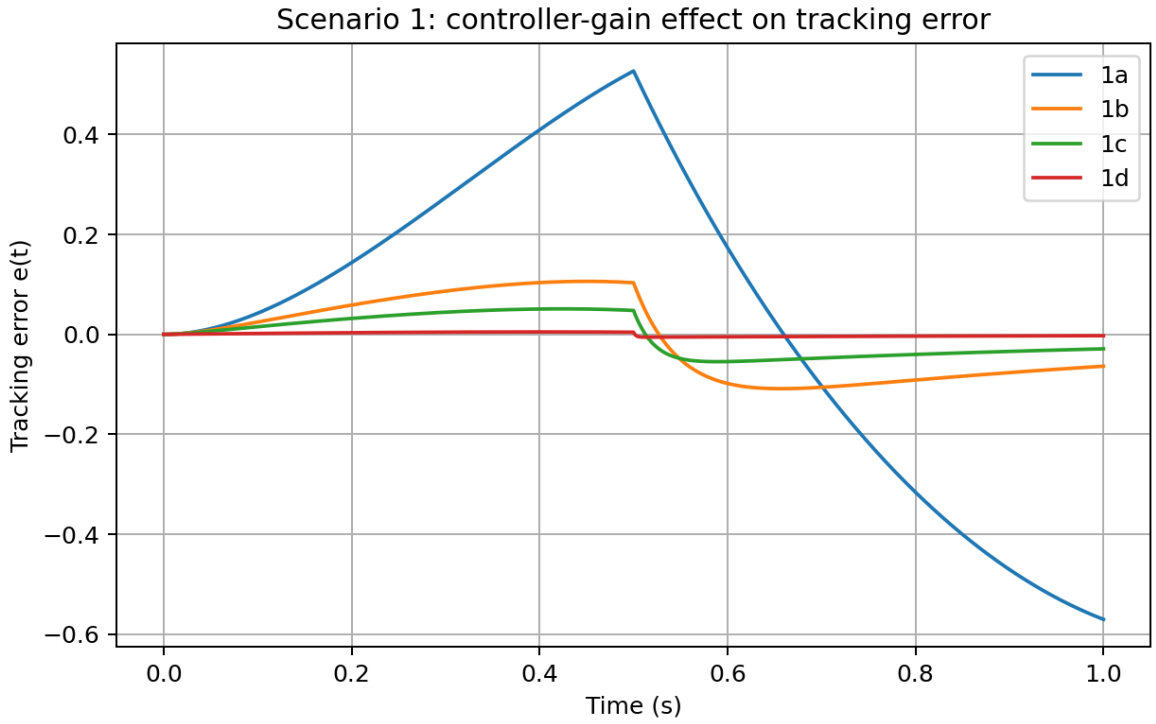


Figure 10. Tracking error for the four PID gain levels.

4.2 Scenario 2 - Effect of Time Step

Scenario definition. The plant, accelerated reference, and highest PID gain set of Scenario 1 are retained. Numerical resolution alone is varied: Δt=10^{-3}, 10^{-4}, 10^{-5},

and 10^{-6} s (1 kHz to 1 MHz). This scenario is a convergence check, not a controller retuning experiment.

Table 6. Convergence with respect to the time step.

ID	dt	fs	Exit	IAE	RMSE	Eu	|u|max
2a	0.001	1000	0.00269817	0.00369885	0.003909	4.24767	3.4982
2b	0.0001	1.0000e+04	0.00270113	0.00369678	0.00390806	4.23762	3.49817
2c	1.0000e-05	1.0000e+05	0.00270143	0.00369667	0.00390806	4.23689	3.49817
2d	1.0000e-06	1.0000e+06	0.00270146	0.00369667	0.00390806	4.23682	3.49817

The principal metrics have practically converged already at 10 kHz. Control energy changes from 4.2477 at 1 kHz to 4.2368 at 1 MHz, while IAE and RMSE change only slightly. The 100 kHz sampling used in the baseline study is therefore sufficient for these time responses, but numerical convergence should be documented from the metrics rather than from spectral ratios at frequencies where the input FFT is nearly zero.

The significance of this result is numerical rather than dynamical. Once the principal time-domain metrics cease to change materially as Δt is reduced, further refinement mainly increases computational cost without altering the engineering conclusion. This convergence check is important because later frequency-domain ratios can be misleading at poorly excited FFT bins; the stable IAE, RMSE, and Eu values provide a more reliable indication that the reported time responses are not artifacts of the selected integration step.

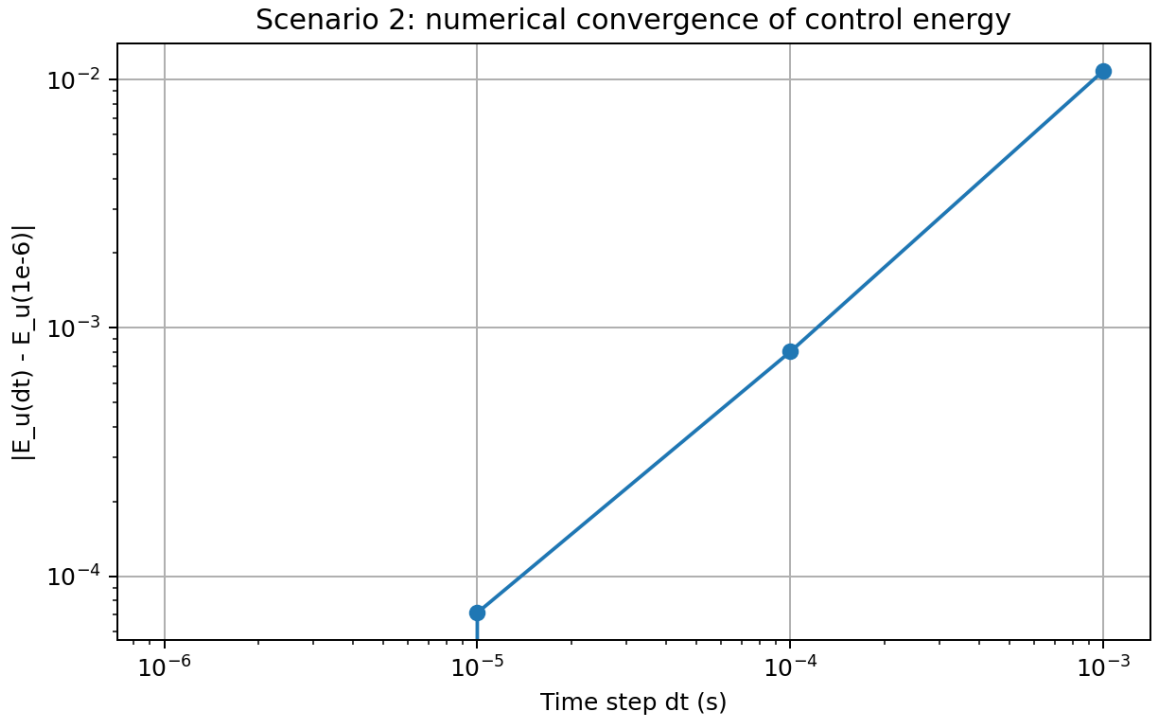


Figure 11. Convergence of control energy with respect to dt.

4.3 Scenario 3 - Effect of Reference Shape/Bandwidth

Scenario definition. The nominal plant and PID are held fixed while four reference classes are applied. All runs have $T = 1$ s, $A = 5$, and $\Delta t = 10^{-5}$ s. The commands implemented in the numerical study are

- **Accelerated command (3a):** $r(t) = At^2$ for $0 \le t < T/2$, followed by the held value $r(t) = A(T/2)^2 = 1.25$ for $T/2 \le t \le T$.
- **Sinusoidal command (3b):** $r(t) = (A/2)\sin(2\pi\, 5t)$ for $0 \le t < T/2$, after which the value attained at $T/2$ is held. With the present T and frequency this held value is zero.
- **Step command (3c):** $r(t) = 0$ for $0 \le t < T/2$ and $r(t) = A = 5$ for $T/2 \le t \le T$.
- **Pulse command (3d):** two rectangular pulses of duration $100\Delta t = 1$ ms are applied: $r(t) = +A$ for $T/4 \le t < T/4 + 1$ ms and $r(t) = -A$ for $T/2 \le t < T/2 + 1$ ms; $r(t) = 0$ elsewhere.

The purpose is to isolate the effect of reference bandwidth and discontinuities on derivative action and control effort. The accelerated and sinusoidal commands are smooth over their active intervals, whereas the step and short pulses introduce broadband, high-rate transitions and therefore deliberately stress the ideal derivative term.

Table 7. Results for different forms of r(t).

ID	Ref	Exit	IAE	RMSE	Eu	|u|max
3a	accelerated	0.00270143	0.00369667	0.00390806	4.23689	3.49817
3b	sinusoidal	0.00182653	0.0514318	0.0783463	1538.61	78.6201
3c	step	0.0311412	0.0321125	0.14745	1.1262e+05	1.0250e+05
3d	pulse	9.0679e-06	0.0137056	0.169214	4.3597e+05	1.0250e+05

The reference waveform strongly affects the required energy. The smooth accelerated signal requires E_u about 4.24, the sinusoid about 1.54×10^3, while the step and narrow pulse produce very large values because of the ideal PID derivative and abrupt transitions. This result establishes that large energy should not be interpreted as a property of the nonlinear FRF, but as a combination of reference bandwidth, controller, and discrete implementation.

The comparison also explains why controller-effort figures cannot be compared independently of the command class. A smooth trajectory contains limited high-frequency content, whereas a step or narrow pulse forces the ideal derivative action to react to abrupt changes. The very large Eu values for discontinuous commands therefore identify a bandwidth/implementation limitation of the controller rather than an intrinsic energy property of $\dot{x}$=x²+u. In an experimental implementation, reference shaping or derivative filtering would be required before such commands could be interpreted physically.

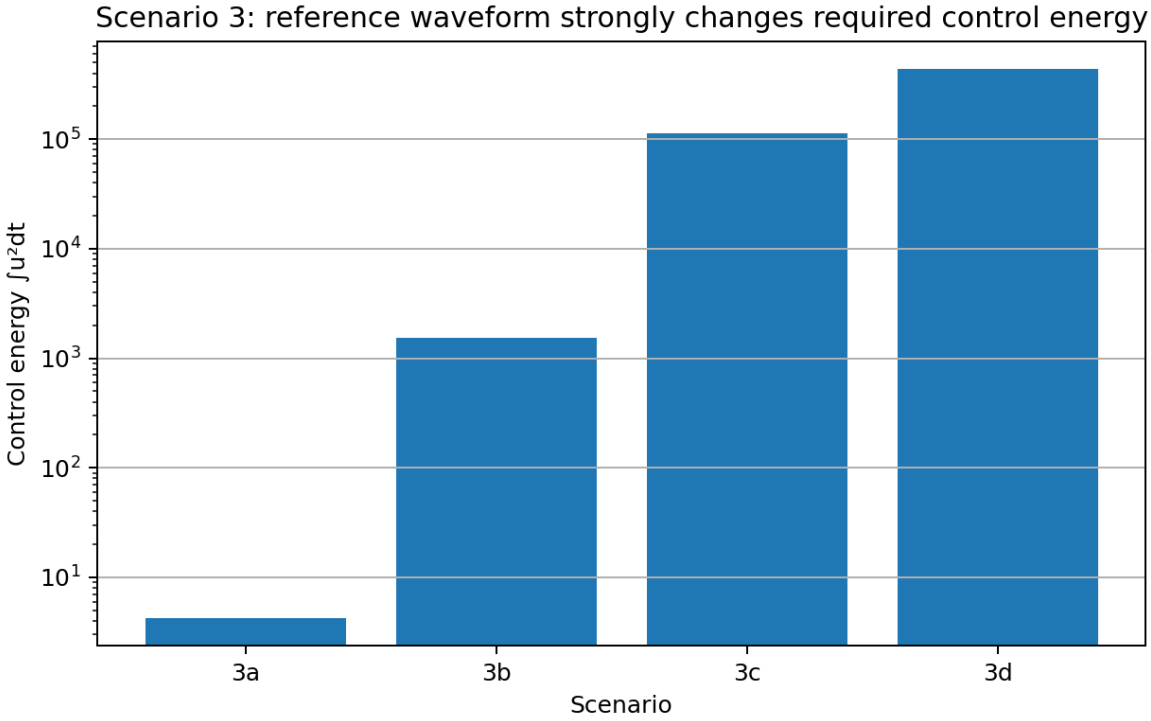


Figure 12. Control energy for the four reference waveforms.

4.4 Scenario 4 - Nonlinearity Order

Scenario definition. The same closed-loop configuration and reference are retained while the plant nonlinearity is changed to $f(x) = x^n$ for every integer order $n = 3, 4, \ldots, 12$. The controller is not reinterpreted as defining a new transfer function; the test compares finite-amplitude tracking and control effort for different polynomial orders.

Table 8. Effect of exponent n on the closed-loop system.

ID	n	Exit	IAE	RMSE	Eu	|u|max
4a	3	0.00309247	0.00401602	0.00426196	5.04641	3.53308
4b	4	0.00356484	0.00438048	0.00468993	6.21129	3.62120
4c	5	0.00414928	0.00482424	0.00524070	8.01959	3.70129
4d	6	0.00487943	0.00538059	0.00596643	10.9136	4.02286
4e	7	0.00579606	0.00610087	0.00693209	15.6278	5.12935
4f	8	0.00694968	0.00705397	0.00822550	23.4350	6.59087
4g	9	0.00840154	0.00831862	0.00997423	36.6417	8.56666
4h	10	0.0102181	0.0100216	0.0123794	59.6843	11.3370
4i	11	0.0124376	0.0123793	0.0157961	101.903	15.4737
4j	12	0.0148951	0.0158058	0.0209798	186.296	22.5103

With a fixed PID and the same trajectory, increasing n does not leave the control problem unchanged. The complete sweep shows a progressive rise in control effort: E_u increases from 5.05 at $n = 3$ through 8.02, 10.91, 15.63, 23.43, 36.64, and 59.68 for $n = 5$ through $n = 10$, then reaches approximately 101.90 and 186.30 for $n = 11$

and $n = 12$, respectively. This contradicts the generalization that different polynomial nonlinearities have essentially the same "transfer function" $1/s$. They may share the same local model $1/s$ at $x_e = 0$ when f'(0)=0, but their finite-amplitude behavior is very different.

This finite-amplitude sweep is the clearest distinction between local and global descriptions in the chapter. Several polynomial models can share the same local integrator-like linearization at $x_e = 0$, yet the now fully resolved $n = 3$–12 sweep shows a smooth but rapidly accelerating increase of control energy with nonlinearity order, confirming that their finite-amplitude trajectories away from the equilibrium are not equivalent. Thus, agreement of local transfer functions is useful only inside the neighborhood in which the linearization is valid; it cannot justify treating different nonlinear orders as the same plant for finite excursions.

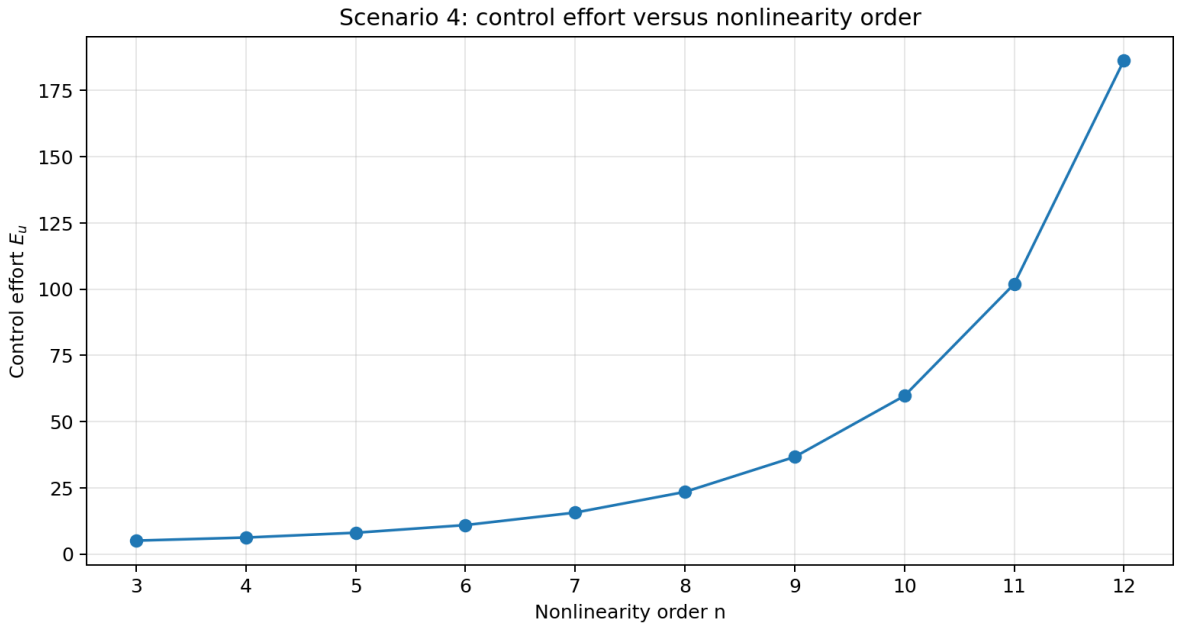


Figure 13. Control energy as a function of nonlinearity order.

4.5 Scenario 5 - Empirical FRF and Amplitude Dependence

Scenario definition. The plant is excited by a random-phase odd-line multisine containing 1,3,...,99 Hz. The total input is normalized to RMS levels 0.1, 1, 5, 10, and 20. The same repeatable phases are used at each level; X/U is evaluated only at excited lines and compared with the local limit $1/(j\omega)$. Even unexcited lines are retained as quadratic-distortion detection lines.

Applied random but repeatable phases and normalization of the total RMS level. The ratio X/U is computed only at excited lines. The curve is compared with the local $P_{\text{lin}}(\text{j}\ \omega;0)=1/(j\omega)$.

Table 9. Dependence of the empirical FRF on excitation level.

RMS(u)	peak|x|	x(T)	Err_mag(dB)	Err_phase(deg)	D_{even}
0.1	0.00777365	1.1587e-05	0.0100092	1.05382	0.000915173
1	0.078347	0.00163947	0.103415	1.35882	0.00943533
5	0.406107	0.0485299	0.602097	4.38376	0.054885
10	0.852335	0.246744	1.55324	10.5414	0.138187
20	2.50358	2.48155	6.22098	77.532	0.497678

For RMS=0.1 the empirical FRF is almost identical to $1/s$: magnitude RMS error is about 0.01 dB and the even-distortion index is 9.15x10^{-4}. When RMS increases to 10, the magnitude error becomes 1.55 dB and the distortion index 0.138. At RMS=20 the deviation is pronounced: 6.22 dB, phase RMS error 77.5 degrees, and D_{even} about 0.498. This is direct numerical evidence that X/U is not a unique transfer function of the nonlinear plant.

The amplitude sweep provides the direct frequency-domain counterpart of the preceding time-domain observation. At small RMS excitation the nonlinear trajectory remains close enough to the operating point that the local $1/s$ model is an excellent approximation. As the excitation grows, the simultaneous increase in magnitude error, phase error, and even-line distortion shows that energy is being redistributed by the quadratic nonlinearity. The empirical X/U ratio is therefore meaningful only together with its excitation amplitude and distortion indicators.

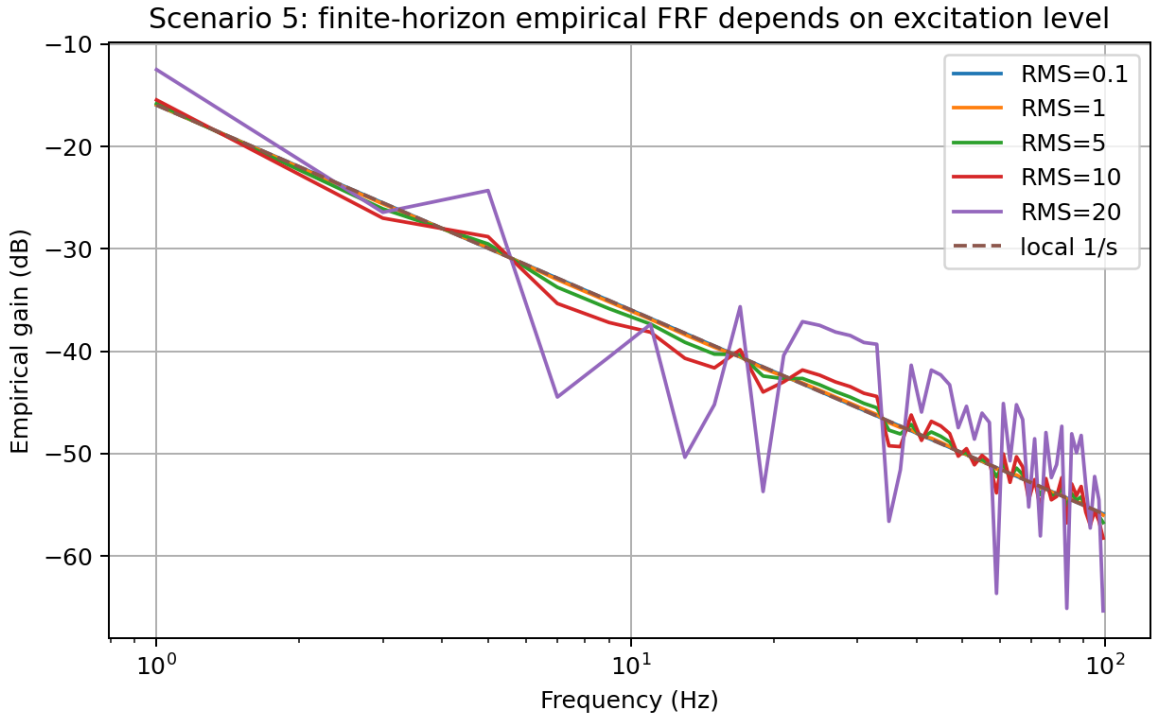


Figure 14. Empirical FRF for different RMS levels and the local $1/s$ limit.

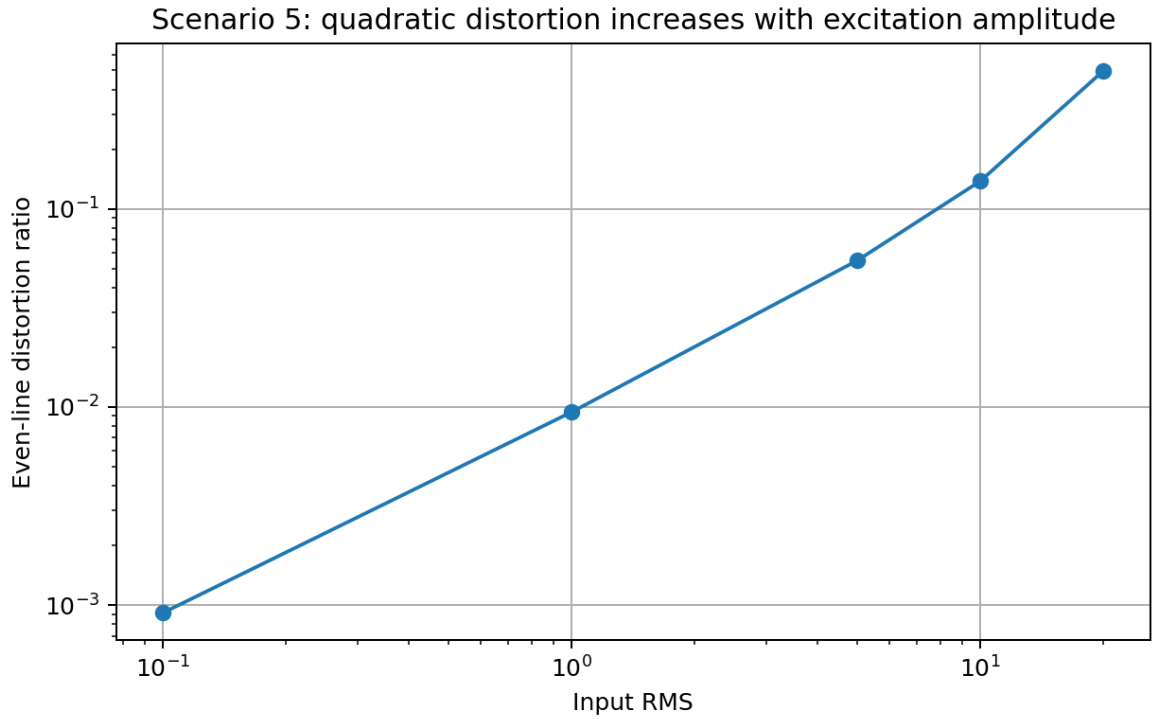


Figure 15. Increase of even nonlinear distortion with excitation level.

4.6 Scenario 6 - Local Stabilizability

Scenario definition. The equilibrium x_e=0.5, u_e=-0.25 of $\dot{x} = x^2 + u$ is perturbed locally. Proportional small-signal feedback δu=-K δx is applied with K=0.5, 1.0, 1.2, and 2.0. Since the local eigenvalue is $\lambda = 1 - K$, the cases intentionally span unstable, marginal/non-asymptotic, and stable local behavior.

The open-loop unstable point x_e=0.5, u_e=-0.25 is examined. For f=x^2, a=2x_e=1. With proportional feedback δu=-K δx, the local eigenvalue is $\lambda = 1 - K$. Theory predicts local stability for K>1.

Table 10. Local stabilizability test at $x_e = 0$.5.

xe	K	lambda	decay	z(T)
0.5	0.5	0.5	0	92.4239
0.5	1	0	0	0.0666667
0.5	1.2	-0.2	1	0.0218464
0.5	2	-1	1	0.000354503

The nonlinear simulation agrees with local theory: K=0.5 leads to escape, K=1 does not provide asymptotic decay because the quadratic term remains, while K=1.2 and K=2 reduce the initial perturbation. The local stabilizability interpretation therefore has a clear mathematical basis as the existence of a controller that stabilizes the selected operating point.

The stabilizability test connects the local pole calculation to the nonlinear state equation. The cases K<1, K=1, and K>1 deliberately straddle the predicted boundary

$\lambda = 1 - K$. The nonlinear trajectories follow the expected local trend, while the K=1 case also shows why a zero linearized eigenvalue cannot be interpreted as asymptotic stability: the neglected nonlinear term becomes decisive. The experiment therefore validates the local criterion without extending it beyond its mathematical scope.

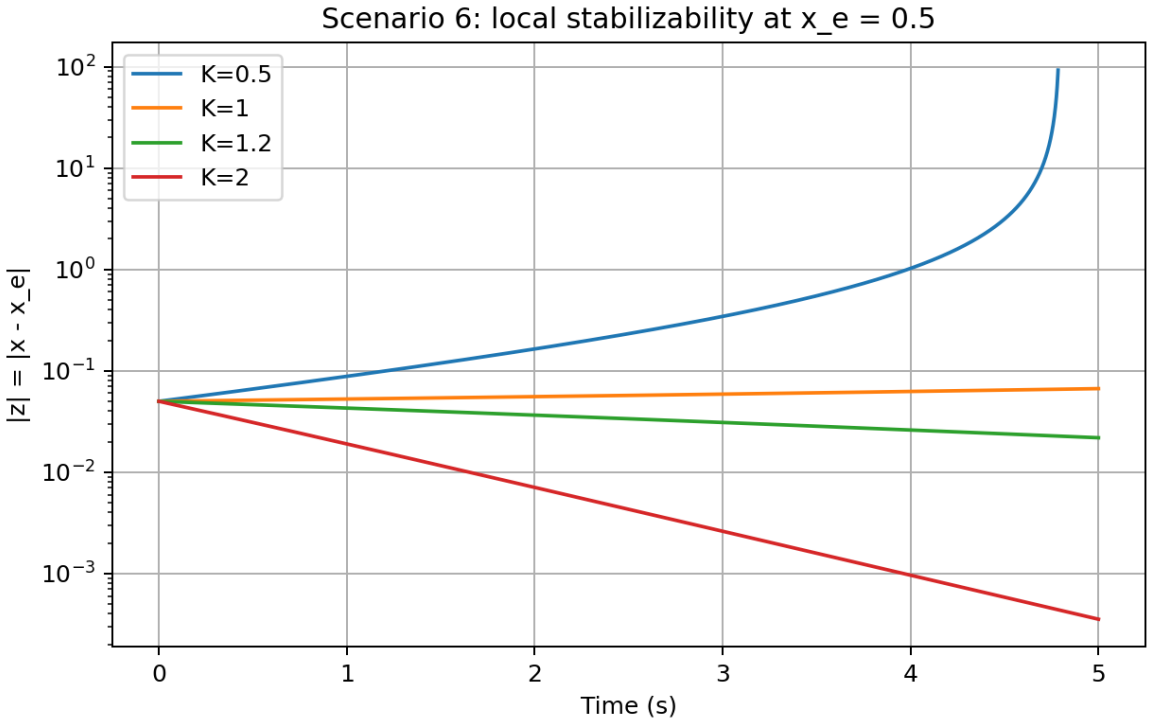


Figure 16. Local perturbation response for different K.

5 Discussion

The results preserve the substantive objective of the study without relying on the invalid concept of a unique global transfer function. Closed-loop behavior can indeed be used to extract a controller-conditioned linear description, but it must be called a local linearization, BLA, or empirical FRF depending on how it is determined. This quantity is not identical to the nonlinear plant as a mathematical object.

The new RMS normalization reveals the expected amplitude dependence and generation of even-frequency components.

The method does not replace generalized nonlinear frequency-domain methods. When a full description of cross-frequency couplings is required, Volterra/GFRF or NARMAX/NOFRF techniques are theoretically more appropriate [6-8]. The present approach targets a narrower practical level: a local model for control design and an empirical FRF for quantifying the extent to which a linear approximation is acceptable in a specified experiment.

6 Conclusions

- A general nonlinear SISO system does not possess a unique classical transfer function independent of excitation and operating point.
- The correct classical description is the local transfer function of the linearization. For $\dot{x} = x^2 + u$, $P_{\text{lin}}(s; x_e)$=1/(s-2x_e), and at $x_e = 0$, P_{lin}=$1/s$.
- The ratio X/U obtained from a finite experiment is an empirical FRF. The new experiments quantitatively demonstrate its dependence on RMS level.

The six scenarios together establish a consistent hierarchy of descriptions. Local linearization explains infinitesimal behavior around a selected equilibrium; empirical FRFs summarize a specified finite experiment; and nonlinear distortion measurements reveal when the linear approximation is losing validity. Controller gains, numerical resolution, reference bandwidth, nonlinear order, excitation amplitude, and operating point each affect a different part of that hierarchy. The chapter therefore supports using frequency-response concepts for nonlinear systems only when the operating condition and the type of linear approximation are stated explicitly.

7 Limitations and Future Work

The empirical FRF in Scenario 5 has a finite time horizon and is not a complete BLA estimate based on multiple random phases with statistical separation of noise and nonlinear distortion. A natural extension is to use random-phase multisine ensembles, robust BLA, and comparison with Volterra or NARMAX models. Practical PID implementations also require a filtered derivative and actuator saturation, especially for step or pulse references.

Relationship to the Complete Book

This paper is a self-contained study extracted and reformatted from the corresponding research chapter of *Nonlinear Control: From Model to Evidence*. The complete book provides the unified progression across all seven studies, cross-study synthesis, extended methodological context, and the MATLAB/Octave and Python software-companion architecture used for replication and further experimentation.

7.1 References

[1] H. K. Khalil, Nonlinear Systems, 3rd ed., Prentice Hall, 2002.

[2] J.-J. E. Slotine and W. Li, Applied Nonlinear Control, Prentice Hall, 1991.

[3] R. Pintelon and J. Schoukens, System Identification: A Frequency Domain Approach, 2nd ed., Wiley-IEEE Press, 2012. DOI: 10.1002/9781118287422.

[4] J. Schoukens, R. Pintelon, Y. Rolain and T. Dobrowiecki, “Frequency response function measurements in the presence of nonlinear distortions,” Automatica, vol. 37, no. 6, pp. 939-946, 2001. DOI: 10.1016/S0005-1098(01)00037-1.

[5] R. Pintelon, M. Schoukens and J. Lataire, “Best Linear Approximation of Nonlinear Continuous-Time Systems Subject to Process Noise and Operating in Feedback,” IEEE Transactions on Instrumentation and Measurement, vol. 69, no. 10, pp. 8600-8612, 2020. DOI: 10.1109/TIM.2020.2987476.

[6] C. M. Cheng, Z. K. Peng, W. M. Zhang and G. Meng, “Volterra-series-based nonlinear system modeling and its engineering applications: A state-of-the-art review,” Mechanical Systems and Signal Processing, vol. 87, pp. 340-364, 2017. DOI: 10.1016/j.ymssp.2016.10.029.

[7] S. A. Billings, Nonlinear System Identification: NARMAX Methods in the Time, Frequency, and Spatio-Temporal Domains, Wiley, 2013. DOI: 10.1002/9781118535561.

[8] R. S. Bayma, Y. Zhu and Z. Q. Lang, “The analysis of nonlinear systems in the frequency domain using Nonlinear Output Frequency Response Functions,” Automatica, vol. 94, pp. 452-457, 2018. DOI: 10.1016/j.automatica.2018.04.030.

[9] W. Liu, Y. Zhang, J. Wu, S. Wang, H. Shao and Y. Yang, “An efficient Volterra series approach for identifying nonlinear system vibration responses to an excitation,” Journal of Vibration and Control, vol. 32, no. 3-4, pp. 522-534, 2026. DOI: 10.1177/10775463241298473.

[10] A. Isidori, Nonlinear Control Systems, 3rd ed., Springer, 1995. DOI: 10.1007/978-1-84628-615-5.

[11] E. D. Sontag, Mathematical Control Theory: Deterministic Finite Dimensional Systems, 2nd ed., Springer, 1998. DOI: 10.1007/978-1-4612-0577-7.

[12] J. Schoukens, R. Pintelon and Y. Rolain, Mastering System Identification in 100 Exercises, Wiley-IEEE Press, 2012. DOI: 10.1002/9781118218532.